ACS APPLIED MATERIALS & INTERFACES

Research Article

www.acsami.org

Inkjet-Printed In_2O_3 Thin-Film Transistor below 200 °C

Jun Seok Lee, Young-Jin Kwack, and Woon-Seop Choi*

Department of Display Engineering, Hoseo University, Asan-si, Chungnam 336-795, Korea

Supporting Information

ABSTRACT: High-performance In_2O_3 thin-film transistors could be prepared by an inkjet-printing method below 200 °C with a single precursor and solvent formulation. The self-combustion reaction took place with the electrical properties of In_2O_3 at a low temperature of 147 °C, which was confirmed by X-ray photoelectron spectroacopy and thermal analysis. The electrical properties after postannealing at 200 °C were as follows: a mobility of 3.98 $cm^2/V{\cdot}s$, a threshold voltage of 1.83 V, a subthreshold slope of 0.4 V/dec, and an on-to-off current ratio of 10^8, which are the best properties by an inkjet process thus far. The positive bias stability was much improved by postannealing, and good negative bias stability was obtained.

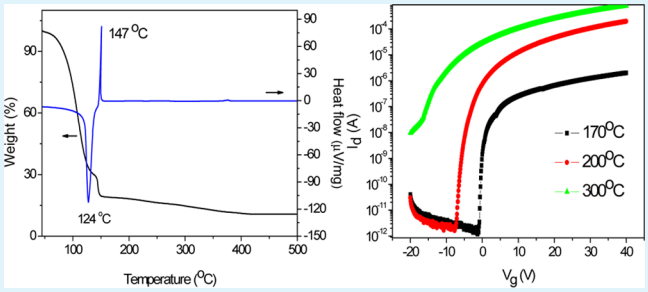

KEYWORDS: *inkjet, low-temperature process, oxide thin-film transistors, indium oxide, combustion*

I. INTRODUCTION

Amorphous oxide semiconductors have been studied as the active channel materials for thin-film transistors (TFTs) in display backplanes and other optoelectronic devices.[1] Many solution-processed oxide semiconductors are based on In_2O_3 and ZnO in binary or tertiary oxide systems, such as InZnO, ZnSnO, and InGaZnO.[2] The properties of these devices are comparable to their vacuum-deposited counterparts, but the annealing temperature for producing metal oxides from the sol–gel solution system generally requires a high temperature because an incomplete reaction below 400 °C causes very poor electrical performance or even no TFT characteristics. Inkjet is an attractive printing technique to prepare a drop-on-demand patterning with large area and mass production for printed electronics. Inkjet printing with accurate control of the drop volume and position enables the production of complex patterns and high-resolution devices without expensive and chemical waste photolithographic processes. Inkjet-printed In–Ga–Zn oxide (IGZO) TFTs prepared from zinc acetate, indium nitrate, and gallium nitrate showed a mobility of 0.05 $cm^2/V{\cdot}s$ at 400 °C after additional 250 °C vacuum annealing.[3] IGZO TFTs with different precursors of zinc acetate, indium chloride, and gallium chloride at 300 and 500 °C postannealing exhibited a mobility of 1.41 $cm^2/V{\cdot}s$.[4] Recently, Hennek et al. demonstrated a mobility of 2.5 $cm^2/V{\cdot}s$ in an inkjet-printed IGZO with bottom contact, bottom gate structure at 400 °C.[5] Marks et al. reported a solution-processed In_2O_3 TFT with different gate dielectrics, silicon dioxide and organic layer.[6] Han et al. reported solution-processed In_2O_3 TFTs by a spin-coating process using a metal halide precursor in acetonitrile and ethylene glycol.[7] Recently, Hahn et al. reported inkjet-printed In_2O_3 TFTs using nanoink-containing In_2O_3 nanoparticles with an electrochemical gate dielectric. This study showed interesting results at room temperature, such as mobilities of 0.8 and 0.26 $cm^2/V{\cdot}s$ for a flat channel organic dielectric and nanowire network, respectively.[8] Galium doping of In_2O_3 thin films allowed a low processing temperature, but the device performance was degraded significantly at 250 °C and the TFT was inactive at 200 °C.[9]

Most multioxide TFTs need high-temperature annealing to obtain good properties. Even though indium is a key element for high mobility in multioxide semiconductors and a strong candidate at low-temperature processing for potential flexible backplane application, few studies have examined In_2O_3 solution-processed In_2O_3 TFTs, and even fewer studies on inkjet-printed In_2O_3 TFTs, because it is not easy to obtain reasonable properties. Until now, most solution-processed oxide thin films for TFT used acetate, chloride, and nitrate precursors with a stabilizer in several solvents to produce a printing process. A low-temperature process was examined using a combustion process, in which an oxide precursor, an oxidant, and a stabilizer were mixed in the solvents.[10] Many chemical species and impurities had a negative effect on the device performance and stability at low-temperature processing.[9] In the present study, a single precursor in a single solvent system, to minimize carbon-based impurities and residuals from the precursor and solvent, was used for a self-combustion In_2O_3 process by optimizing the inkjet process. To the best of our knowledge, this is the first report of inkjet-printed In_2O_3 TFTs with good characteristics at relatively low temperatures (≤200 °C).

II. EXPERIMENTAL SECTION

A bottom-gate and top-contact device structure was used for inkjet-processed In_2O_3 TFT preparation. As a precursor for the semiconductor

Received: July 1, 2013
Accepted: October 22, 2013
Published: October 22, 2013

active layer, 0.3 M indium nitrate hydrate was dissolved in 2-methoxyethanol to form a sol–gel solution mixture, and the solution was stirred at room temperature for 1 h without adding other chemicals. A piezoelectric inkjet printing system (Ommijet Mini-100, Unijet) with 50 μm orifice size was used. Uniform inkjet droplet ejection was achieved by applying a 60 V pulse at a frequency of 500 Hz, substrate temperatures ranging from room temperature to 60 °C, and a nozzle distance of 0.5 mm. A 300-nm-thick thermally grown silicon oxide gate insulator on a heavily doped silicon wafer was treated with O_2 plasma at a radio-frequency power of 200 W for 20 min. After inkjet printing of an indium precursor solution on the silicon oxide gate insulator, the film was dried at 150 °C for 1 min to evaporate the solvent and then annealed thermally at temperatures from 170 to 300 °C for 1 h in air. Aluminum as a source and drain was deposited by thermal means to make a channel width of 1500 μm and a length of 100 μm. Then, the devices were postannealed at temperatures from 170 to 300 °C in air. All current voltage (I–V) characterizations were carried out using a semiconductor parameter analyzer (Keithley 4200) in a dark box under air at room temperature. X-ray photoelectron spectroscopy (XPS; Thermo VG ESCA Sigma Probe) were performed at 15 kV and 100 W using a monochromatic Al Kα radiation source using the C 1s peak (285 eV) for calibration. For Fourier transform infrared (FTIR; Perkin-Elmer Spectrum GX) spectroscopy, the film was prepared on a silicon wafer at temperatures ranging from 170 to 300 °C. Thermal analysis (Mettler Toledo model 851) was performed at a scan rate of 10 °C/min under N_2. The surface topology was examined by atomic force microscopy (AFM; Park System, SE-70) in noncontact mode.

III. RESULTS AND DISCUSSION

III.1. Inkjet-Printed Indium Oxide Films. The concentration of a jetting solution and jetting parameters were optimized to obtain proper jetting In_2O_3 thin films. The surface tension and viscosity of the precursor solution for inkjet were 28.34 dyn/cm and 2.08 cP, respectively. The drying of an inkjet-printed droplet can be controlled by substrate heating to produce a good spread for a uniform film with suitable thickness. Single droplets were analyzed using a surface profiler, as shown in Figure 1. The droplet was injected at range of

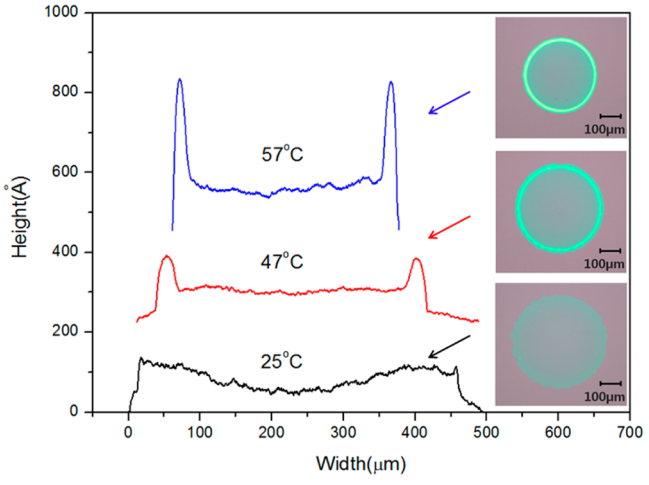

Figure 1. Surface profiles of single dots of inkjet-printed In_2O_3 at substrate temperatures of 25, 47, and 57 °C.

substrate temperatures, 25, 47, and 57 °C. With increasing preheated substrate temperature, the droplet showed outer ring formation, a so-called coffee-ring effect. The droplet spread out on the substrate, and the center layer was then pinned. This coffee-ring effect can be suppressed by rapid heating to evaporate the solvents before the onset of hydrodynamic flow.

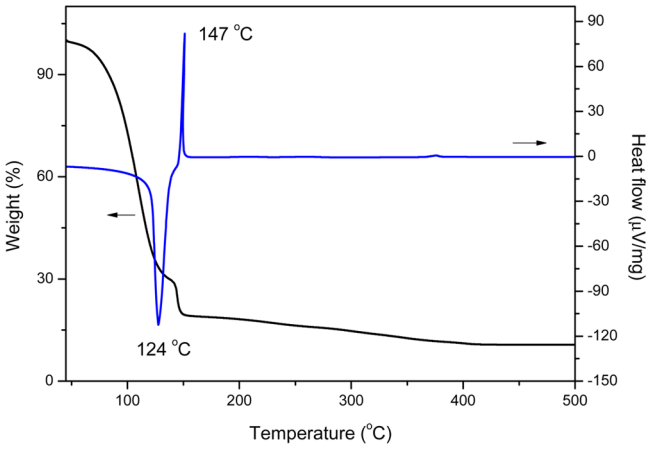

Figure 2. DTA/TGA thermogram of a In_2O_3 precursor solution at a scan rate of 10 °C.

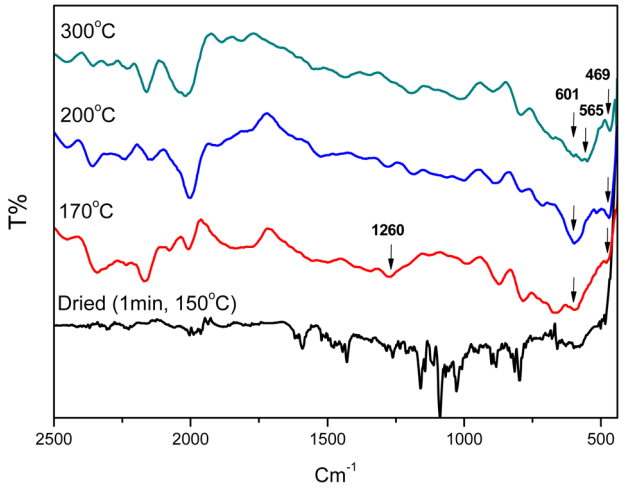

Figure 3. FTIR analysis of inkjet-printed In_2O_3 thin films at processing temperatures of 170, 200, and 300 °C.

Several surface treatments with self-assembled monolayers to have hydrophobicity could also control the coffee-ring effect, but the properties of the device did not show any improvement.[11] In the present case, the boiling point of the solvent, 2-methoxyethanol, is higher than that of a common inkjet solvent, acetonitrile.[12] Two conditions, contact line pinning and evaporation from the edge, are necessary for ring formation. The surface tension decreased with increasing substrate temperature, and the surface tension would be highest at the top of the drop. This gradient would drive a radially inward surface flow.[13] Therefore, higher substrate temperatures produce more coffee-ring-affected droplet patterns. This coffee-ring effect was minimized by the leveling of multijetting drops, as shown in AFM and in Figure S1 in the Supporting Information (SI). In the preparation of the inkjet process of In_2O_3, the use of a medium-boiling-temperature solvent was effective in obtaining uniform films. At low substrate temperatures, the thicker precursor layer allowed slow evaporation throughout the precursor/air interface. A large droplet formed with a height of 10 nm and a diameter of 450 μm. At a substrate temperature of 47 °C, the outer ring size was 15 nm in height and 350 μm in inner diameter. The ring size with higher temperature was smaller than that with lower temperature, having 20 nm height and 300 μm diameter. The thickness of

dx.doi.org/10.1021/am4025774 | ACS Appl. Mater. Interfaces 2013, 5, 11578–11583

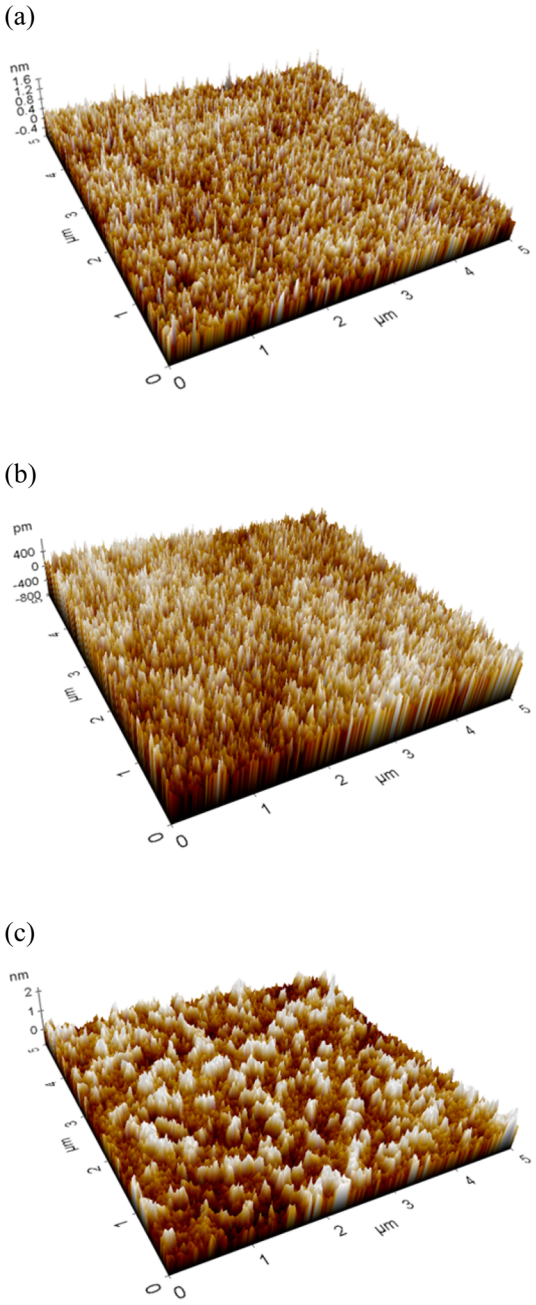

Figure 4. AFM topology of the active layer in inkjet-printed In_2O_3 TFT after postannealing at (a) 170, (b) 200, and (c) 300 °C.

the droplet was 12 nm at low temperature, which increased with increasing substrate temperatures.

The thermal behavior of the inkjetted In_2O_3 thin film was analyzed by differential thermal analysis (DTA)/thermogravimetric analysis (TGA), as shown in Figure 2. There was a rapid decomposition exothermic peak of organic compounds at 147 °C after solvent evaporation at 124 °C. In our In_2O_3 system, self-combustion was observed at this point without additional fuel and oxidizer. This lowest self-combustion could be achieved by higher indium loading (0.3 M) and the fueling role of 2-methoxyethanol. The reported combustion process had lower indium loading with additional chemicals.[10] There was a small exothermic peak over 300 °C, which might be additional metal oxide formation from the remaining chemicals and crystallization. The indium nitrate precursor began to decompose at approximately 147 °C by self-combustion and decomposed completely at 250 °C in TGA. Ligand exchange started between the nitrate precursor and 2-methoxyethanol at low temperatures, and metal alkoxide condensation occurred to form a partial network of metal−oxide bonds at elevated temperatures. The XRD pattern showed a (222) crystalline orientation at 31° at over 200 °C annealing samples but is amorphous at 170 °C samples in Figure S2 in the SI.

The chemical configuration of dried and annealed In_2O_3 films was analyzed by FTIR at a range of temperatures, as shown in Figure 3. There were organic residuals in the dried In_2O_3 film due to incomplete decomposition. No 2-methoxyethanol peak was observed for all of the annealed In_2O_3 because of its lower boiling point (125 °C) than the annealing temperatures. The bending vibration of the metal−oxide peak at 1260 cm^{-1} was observed in a dried (unannealed) film and at a 170 °C annealed film, which was assigned to indium methoxyethanol complexes. The peak disappeared gradually with increasing temperature. As the temperature was increased from 170 to 300 °C, the In−O phonon vibration bonding peaks appeared at low-wavelength bands, 469, 565, and 601 cm^{-1}, which were characterized in cubic In_2O_3.[14] Figure 4 showed the surface morphology at various annealing temperatures determined by AFM. R_q (root-mean-square roughness) and R_a (average roughness) were 0.182, 0.184, and 0.277 nm and 0.141, 0.145, and 0.214 nm at annealing temperatures of 170, 200, and 300 °C, respectively. The surface roughness data suggested that this inkjet-printed In_2O_3 thin film was quite smooth and uniform.

XPS analyses were performed on inkjet In_2O_3 thin films. Figure 5 presented the atomic concentration of the inkjet films as a function of the sputtering time for XPS depth analysis. The amount of indium, In $3d_{5/2}$, and oxygen, O 1s, increased with increasing annealing temperature. The XPS oxygen peak was fitted using a Gaussian method to deconvolute the peak into three peaks, 529.8, 531.3, and 532.3 eV. Interestingly, the In_2O_3 films annealed at 170 and 200 °C showed oxide lattice formation and oxygen vacancies with a hydroxyl peak. In Figure 5d for In_2O_3 at the 170 °C process, the dominant peak of the O 1s XPS spectrum at 529.8 eV (O_{OXY}) was assigned to the oxygen atoms in the fully oxidized indium surroundings. The midpeak at 531.3 eV (O_{VAC}) is associated with the oxygen ions in the oxygen-deficient region, i.e., oxygen vacancies. The peak with a high binding energy at 532.3 eV (O_{OH}) indicated the presence of loosely bound oxygen associated with H_2O and OH groups on the surface. The amounts of O_{OXY}, O_{VAC}, and O_{OH} were 52.25, 34.02, and 13.73%, respectively. The fraction of metal−oxide bonding increased with temperature, whereas the fraction of oxygen vacancies and bounded hydroxyl decreased in Figure S3 in the SI. The formation of an oxygen lattice and oxygen vacancies revealed the electric properties of In_2O_3 at low-temperature processing.

III.2. Inkjet-Printed Indium Oxide TFTs. In solution-processed In_2O_3 TFTs, ethanolamine as a base played a critical role in the TFT performance, and a base-free formulation showed low mobility after 400 °C annealing.[7] Owing to the conducting characteristics of In_2O_3, doping is necessary for controlling excess carrier generation.[9] In the inkjet process, the jetting voltage was also an important factor for electrical characteristics, as shown in Figure S4 in the SI. Because a lower jetting voltage gave uneven film formation and a higher jetting voltage produced too thick films with shifting of the transfer curves, the optimized jetting voltage was 60 V for this system. Without additives, the transfer characteristics of an inkjet-printed In_2O_3 TFT could be obtained even at a low annealing

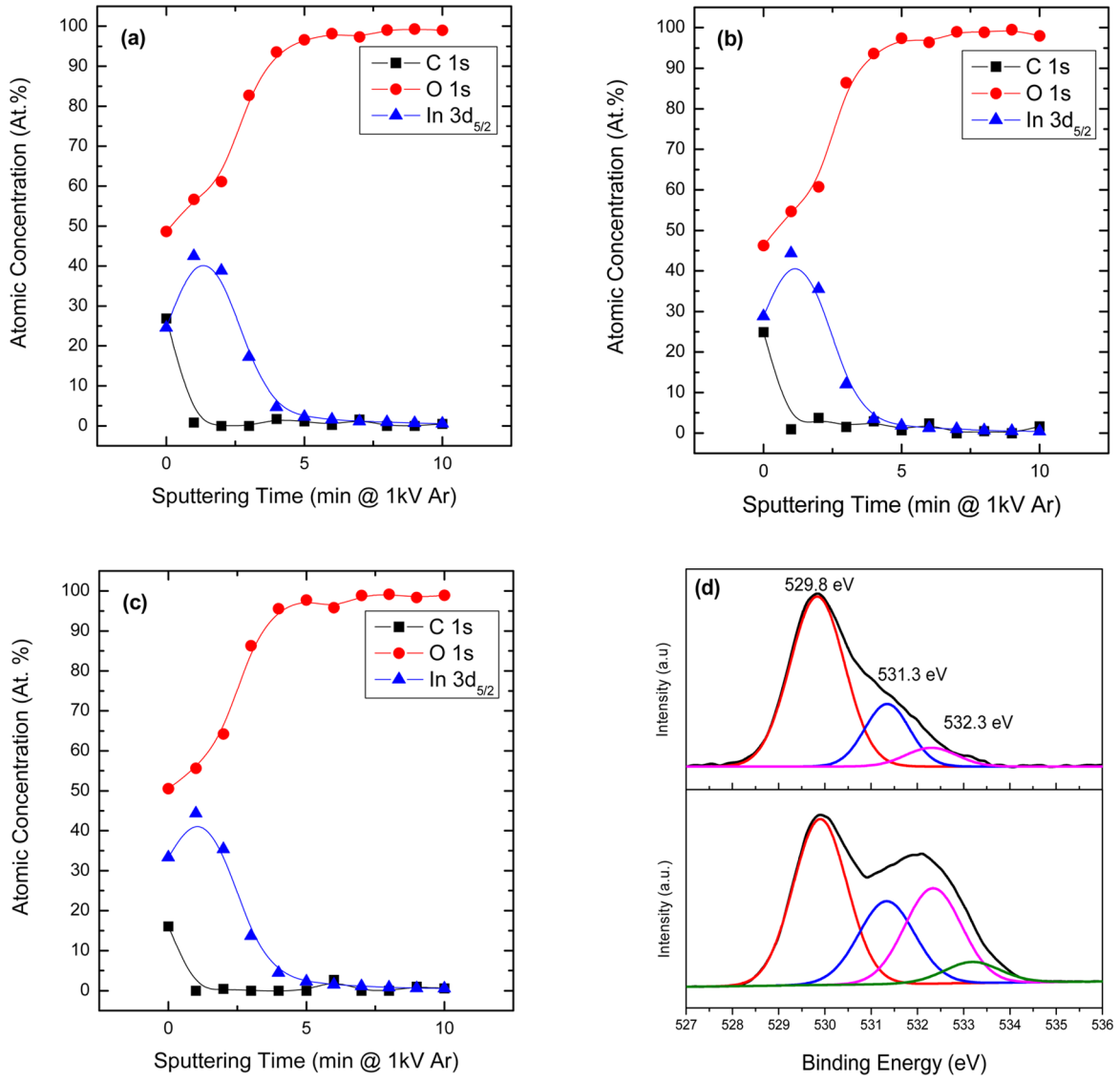

Figure 5. XPS depth profile of inkjet-printed In_2O_3 with temperatures of (a) 170, (b) 200, (c) 300 °C and O 1s core peaks (d) at 170 °C (top) and just dried (bottom).

Table 1. Electrical Properties of Inkjet-Printed In_2O_3 TFTs at Various Annealing Temperatures

annealing temp (°C)	substrate temp (°C)	mobility ($cm^2/V{\cdot}s$)	I on/off	subthreshold slope (V/dec)	V_{th} (V)
170	47	0.016	1.34×10^6	0.3	2.0
200	47	1.83	$\sim 10^8$	0.3	−1.9
300	47	6.27	8×10^4	3.0	−5.7

temperature of 170 °C, as shown in Table 1 and Figure 6a. The transfer properties of an inkjet-printed In_2O_3 TFT at 170 °C showed a mobility of 0.016 $cm^2/V{\cdot}s$, a threshold voltage of 2 V, and a subthreshold slope of 0.3 V/dec. The mobility improved with increasing annealing temperature, 1.83 and 6.27 $cm^2/V{\cdot}s$ at 200 and 300 °C, respectively. The annealing temperature has a huge impact on the electrical properties of TFTs as mentioned above. Improved electrical properties of inkjet-printed In_2O_3 TFTs could be obtained by postannealing in Table 2. After postannealing at 170 °C, the inkjet-printed In_2O_3 TFTs showed improved electrical properties, such as a mobility of 0.11 $cm^2/V{\cdot}s$, a threshold voltage of −1.7 V, and a subthreshold slope of 0.8 V/dec. After postannealing at 200 °C, the electrical properties also showed considerable improvement, a reasonable mobility of 3.98 $cm^2/V{\cdot}s$, a threshold voltage of 1.83 V, and a subthreshold slope of 0.4 V/dec. The operation mode of the TFTs was changed from an enhancement mode to a depletion mode with increasing annealing temperature. The observed left shift in V_{th} is due to higher intrinsic carrier concentrations for films annealed at higher temperatures and due to fewer lattice defects acting as electron traps. In inkjet-processed oxide TFTs, transfer curves were negatively shifted and V_{th} was negative with a thick active layer because the TFT was partially depleted under a zero gate bias.[4] The output characteristics in Figure 6b showed good contact, a clear pinch-off, and solid saturation, indicating that inkjet-printed In_2O_3 TFTs followed the standard field-effect transistor theory.

dx.doi.org/10.1021/am4025774 | ACS Appl. Mater. Interfaces 2013, 5, 11578−11583

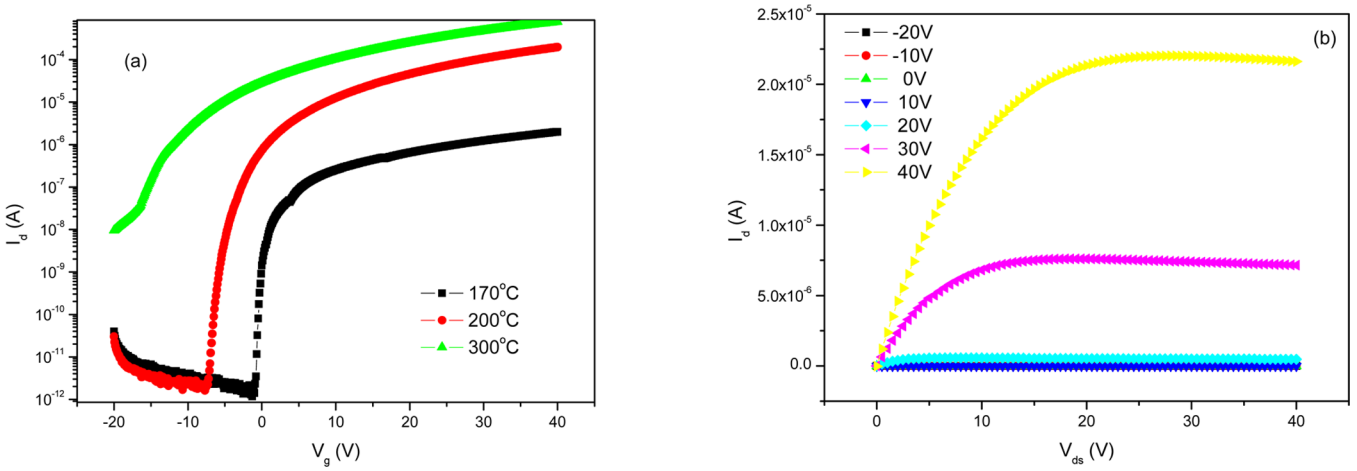

Figure 6. (a) Transfer characteristics with temperatures and (b) output characteristics at 200 °C of an inkjet-printed In_2O_3 TFT before postannealing.

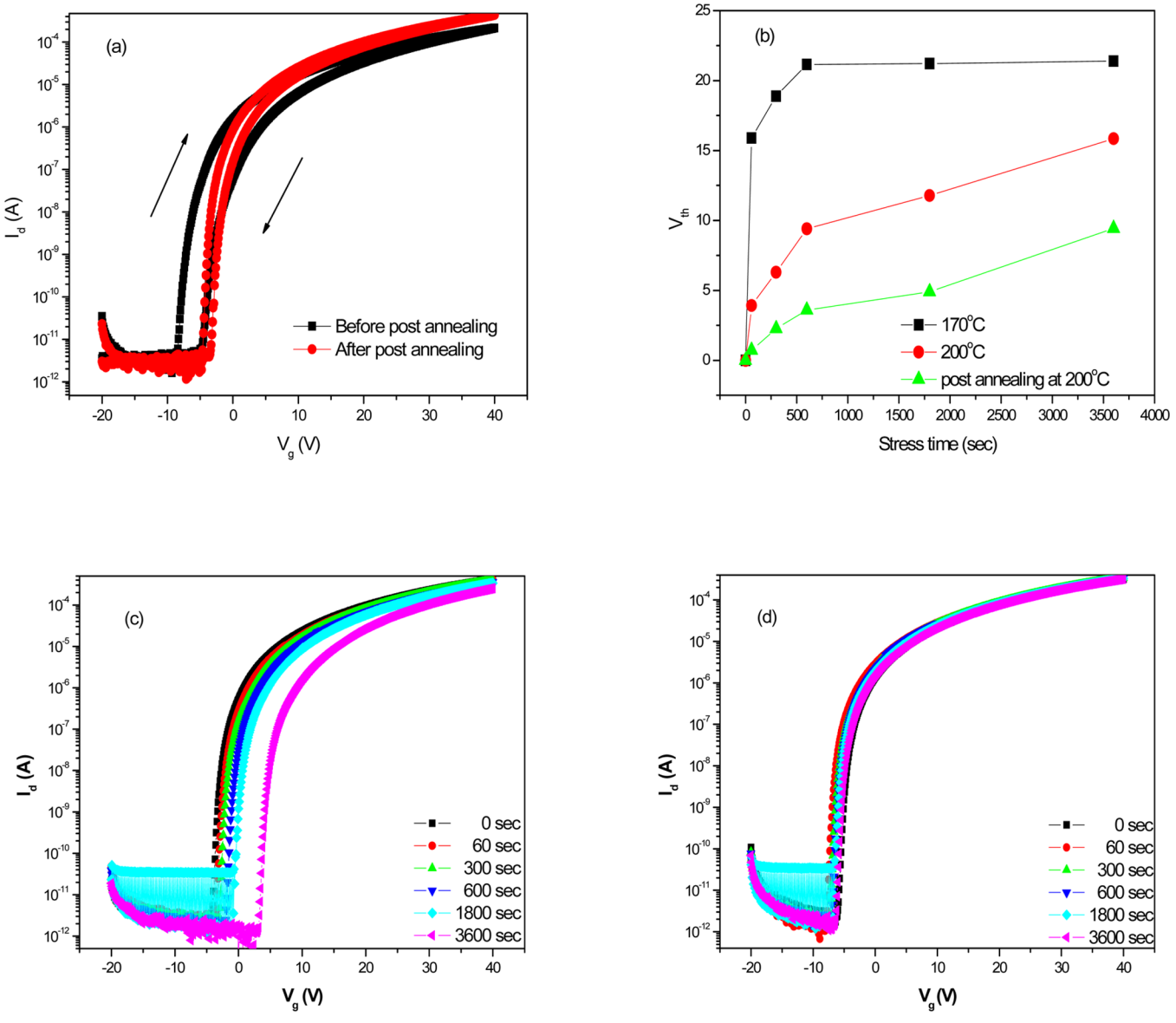

Figure 7. Electrical properties of an inkjet-printed In_2O_3 TFT after 200 °C postannealing: (a) hysteresis behavior before and after postannealing; (b) V_{th} shift after positive bias stress; (c) transfer characteristics after positive bias stress; (d) transfer characteristics after negative bias stress.

dx.doi.org/10.1021/am4025774 | ACS Appl. Mater. Interfaces 2013, 5, 11578−11583

Table 2. Postannealing Effect on the Electrical Properties of Inkjet-Printed In_2O_3 TFTs

postannealing temp (°C)	substrate temp (°C)	mobility ($cm^2/V{\cdot}s$)	I on/off	subthreshold slope (V/dec)	V_{th} (V)
170	47	0.11	6.58×10^6	0.8	−1.72
200	47	3.98	1.66×10^8	0.4	1.83

Figure 7a shows the hysteresis behavior of an inkjet-printed In_2O_3 TFT at 200 °C. Large hysteresis behavior with a 4.2 V voltage shift at the low-temperature process was observed, but the hysteresis decreased to a 1.2 V voltage shift after post-annealing. The presence of clockwise hysteresis is consistent with electron trapping at or near the interface between the oxide semiconductor and gate dielectric or within the semiconductor channel layer.[15] The TFTs were gate-bias-stressed under positive bias stress of V_g = 20 V and negative bias stress of V_g = −20 V for 3600 s. The transfer characteristics under positive bias stress were analyzed as shown in Figure 7b,c. The transfer curve of the inkjet-printed In_2O_3 TFT under bias stress positively shifted with time. The positive V_{th} shift with a positive bias voltage resulted from a negative charge trapped at the interface of the channel and dielectric or injected into the gate dielectric.[16] Because unfinished metal−oxide networking and residual chemical species provide readily available trap sites in the channel region and interface at low processing temperatures, the V_{th} shift was relatively large at the early stages. After charge trapping, the shift in V_{th} became saturated with time. As the process temperature increased, there was a smaller voltage shift due to less charge trapping in the channel and interface regions. In the case of an inkjet-printed In_2O_3 TFT at 200 °C, the bias stability was improved dramatically by postannealing in Figure 7b. No significant charge trapping of the carriers with very similar subthreshold slopes was obtained by post thermal annealing. Postannealing provided more metal−oxide formation, improved contact, and denser film formation by reducing the defects and traps, which might affect the electrical properties of TFTs. The microstructures of the In_2O_3 thin films were barely observed by SEM and TEM. Because the change in the subthreshold slope was negligible during the bias stability test, the possibility of defect formation and deep traps inside the In_2O_3 semiconductor was neglected. Charge trapping at the interface of the semiconductor and dielectric and/or in the gate dielectric is the main mechanism of the V_{th} instability. Figure 7d shows transfer curves of the In_2O_3 TFTs with postannealing at 200 °C after negative bias stress. The negative shift of V_{th} under negative bias stress could be attributed to the trapping of hole carriers and an ambient environmental effect. When negative gate-bias stress was applied, the negative shift of V_{th} was not significant because of the depletion state of the electrons at the interface of the dielectric/semiconductor and in the semiconductor channel under negative bias stress. Hole trapping can be disregarded under negative gate-bias stress because oxide semiconductors have a few holes in the balance bands.[17]

IV. CONCLUSION

In conclusion, the In_2O_3 formulation, substrate temperatures during the inkjet process, and postannealing effects were investigated for a low-temperature inkjet process. An optimum substrate temperature and an annealing temperature were 47 and 200 °C, respectively. Thermal analysis and FTIR confirmed that the self-combustion chemical reaction started at approximately 147 °C, and In−O phonon vibration bonding was detected after annealing. From XPS, In_2O_3 films annealed at 170 °C contained oxide lattice formation and oxygen vacancies with a hydroxyl peak, which proves the electrical properties of In_2O_3 TFT at low-temperature processing. After postannealing at 200 °C, considerable improvement in the electrical properties and positive/negative bias stability was obtained.

■ ASSOCIATED CONTENT

Supporting Information

Optical microscopic image, XRD analysis, O 1s XPS spectra, and the effect of inkjetting voltages on the transfer characteristics. This material is available free of charge via the Internet at http://pubs.acs.org.

■ AUTHOR INFORMATION

Corresponding Author

*Phone: +82-41-540-5924. E-mail: wschoi@hoseo.edu.

Notes

The authors declare no competing financial interest.

■ ACKNOWLEDGMENTS

This work was supported by the Basic Science Research Program through the NRF funded by the Ministry of Education, Science and Technology (Grant 2012-039948) and a SAIT (Samsung Advanced Institute and Technology, Samsung Electronics Co., Ltd.) research fund.

■ REFERENCES

(1) Facchetti, A.; Marks, T. J. *Transparent Electronics*; John Wiley & Sons Ltd.: Chichester, U.K., 2010; Chapter 2.
(2) Jeong, S.; Moon, J. *J. Mater. Chem.* **2012**, *22*, 1243−1250.
(3) Kim, D.; Jeong, Y.; Koo, C.; Song, K.; Moon, J. *Jpn. J. Appl. Phys.* **2010**, *49*, 05EB06-1−05EB06-4.
(4) Wang, Y.; Sun, W.; Goh, G. K. L.; Demir, H.; Yu, H. *IEEE Trans. Electron Devices* **2011**, *58*, 480−485.
(5) Hennek, J. W.; Xia, U.; Everaerts, K.; Hersam, M. C.; Facchetti, A.; Marks, T. J. *ACS Appl. Mater. Interfaces* **2012**, *4*, 1614−1619.
(6) Kim, H. S.; Byrne, P.; Facchetti, A.; Marks, T. J. *J. Am. Chem. Soc.* **2008**, *130*, 12580−12581.
(7) Han, S.-Y.; Herman, G.; Chang, C.-H. *J. Am. Chem. Soc.* **2011**, *133*, 5166−5169.
(8) Dasgupta, S.; Kruk, R.; Mechau, R.; Hahn, H. *ACS Nano* **2011**, *5*, 9628−9638.
(9) Jeong, S.; Lee, J.; Lee, S.; Choi, Y.; Ryu, B.-H. *J. Phys. Chem. C* **2011**, *115*, 11773−11780.
(10) Kim, M.; Kanatzidis, M.; Facchetti, A.; Mark, T. *Nat. Mater.* **2011**, *10*, 382−388.
(11) Kim, D.; Jeong, Y.; Song, K.; Park, S.; Cao, G.; Moon, J. *Langmuir* **2009**, *25*, 11149−11154.
(12) Lee, D.-H.; Han, S.-Y.; Hermane, G. S.; Chang, C.-H. *J. Mater. Chem.* **2009**, *19*, 3135−3137.
(13) Robert, D.; Deegan, R. D.; Bakajin, O.; Dupont, T. F.; Huber, G.; Nagel, S. R.; Witten, T. A. *Phys. Rev. E* **2000**, *62*, 756−765.
(14) Robins, J. W. *Practical Handbook of Spectroscopy*; CRC Press: Boca Raton, FL, 2000; p 533.
(15) Wager, J. F.; Keszler, D. A.; Pesley, E. *Transparent Electronics*; Springer-Verlag: New York, 2008; Chapter 5.
(16) Matters, M.; Leeuw, D.; Herwig, P.; Brown, A. *Synth. Met.* **1999**, *102*, 998−999.
(17) Suresh, A.; Muth, J. *Appl. Phys. Lett.* **2008**, *92*, 033502.